

An Investigation into the Influence of the Airflow Path on the Convective Heat Transfer for an Eddy Current Retarder Turntable

Yunfei Liao^{1,*} and Jin Liu²

¹Chongqing Industry Polytechnic College, Chongqing, 401120, China

²Shenzhen Terca Technology Co., Ltd., Shenzhen, 518110, China

*Corresponding Author: Yunfei Liao. Email: liaoyunfei@foxmail.com

Received: 11 November 2019; Accepted: 24 August 2020

Abstract: In order to improve the convective heat transfer relating to an eddy current retarder, the finite element model has been used to assess the performances of different possible designs. In particular, assuming the steady running state of retarder as the working condition, flow and temperature fields have been obtained for the rotor. The influence of airflow path on heat dissipation has been analysed, and the influence of the temperature field distribution on the performance of retarder has been discussed accordingly. The results show that when the steady running state of the turntable is considered, the maximum temperature is lower, the level of turbulence flow is mitigated, and the temperature distribution becomes more regular. These factors contribute to improve the heat dissipation ability of the retarder.

Keywords: Eddy current retarder; turntable; flow field; convection heat transfer

1 Introduction

The number of people and total quantity of goods transported by automobiles have increased rapidly in the past several years, leading to inherent safety issues [1,2]. An eddy current retarder is being widely employed as an auxiliary braking device in vehicles [3,4]. This type of retarder has a rotor disk made of a ferromagnetic material. The working principle involves converting the kinetic energy of a vehicle into heat energy in the excitation magnetic field and radiating it to the surrounding air [5,6]. The heat generated by braking is greater than the heat dissipated, causing a sharp increase in the rotor disk temperature [7]. When a vehicle is in motion, the stator and rotor are the main components of the retarder that are associated with heat dissipation [8]. The stator heat is mainly radiated to the periphery, and a major proportion of this heat is carried away by radiation, the radiating capacity of the retarder is determined by the volume and surface area of the stator [9]. Once the weight of the retarder is determined, its radiation and heat dissipation capacity will not change significantly, and the convective heat transfer due to rotor rotation will have a significant influence on the heat dissipation performance of the retarder [10].



This work is licensed under a Creative Commons Attribution 4.0 International License, which permits unrestricted use, distribution, and reproduction in any medium, provided the original work is properly cited.

2 Theoretical

The objective of this study was to analyse the heat transfer mechanism of a retarder, which transfers heat between the outer surface of the rotor and the surrounding, mainly through convection. The heat quantity is calculated using Newton's law of cooling [11]:

$$Q_{convection} = hA(T_w - T_f)\Delta r \quad (1)$$

where h is the convective heat transfer coefficient ($W/(m^2 \cdot ^\circ C)$); T_w and T_f are the external surface temperature of the turntable and the external swept fluid temperature ($^\circ C$), respectively.

Eq. (1) fundamentally defines only the heat transfer coefficient, and the essential simplification of the convection heat transfer process is not proposed. Heat is transferred by two modes: conduction and convection [12]. The factors influencing these modes, including the origin of flow, state of flow, physical properties of the fluid, phase change, and geometric parameters of the wall, affect the convective heat transfer process [13]. The relationship between the influencing factors and the convective heat transfer coefficient can be expressed mathematically, and the general equation for convective heat transfer without phase change is as follows [14]:

$$h = f(\rho, c_p, \eta, \lambda, u, l) \quad (2)$$

where ρ , η , and u represent the density, dynamic viscosity, and velocity of the swept air, respectively; λ and c_p are the thermal conductivity and specific heat of the brake drum material, respectively; l is the geometric characteristic dimension of the outer surface of the brake drum.

The rotor temperature distribution is influenced by the heat conducted due to the convection of the iron core, stator material, and surrounding air, as well as by factors such as the air gap and rotor speed. Thus, the heat flux through the stator surface is given by:

$$q_c = h_c(T)(T - T_e) \quad (3)$$

where q_c , h_c , and T_e represent the heat flux generated by convection, heat transfer coefficient, and ambient temperature, respectively.

The heat conduction equation for the rotor under the boundary condition is as follows:

$$q_r = h_r(T)(T^4 - T_e^4) \quad (4)$$

$$-\lambda \frac{\partial T}{\partial n} = \varepsilon \sigma F^*(T^4 - T_e^4) \quad (5)$$

where n , ε , σ , and F^* represent the normal vector of the stator boundary, thermal emissivity, Stefan-Boltzmann coefficient, and thermal radiation angle coefficient, respectively.

Because the eddy current loss serves as the heat source, which is mainly due to the skin effect in the stator, the heat generation rate Q is used to analyse the temperature field distribution on the stator.

$$Q = \frac{P}{V} \quad (6)$$

where P is the braking power of the retarder, and V is the volume associated with the skin depth.

3 Numerical Analysis

Designing and improving the retarder is costly and time-consuming. Computational fluid dynamics (CFD) focuses on flow field analysis, whereby we can theoretically obtain the distributions of air flow

field and air velocity at various positions [15]. The mechanical structure design of a turntable can be made, and the design efficiency can be improved based on the CFD analysis results [16]. Therefore, in this study, the two cases of a retarder turntable are analysed using CFD.

3.1 Physical Models and their Design Comparison

The retarder is mounted on the chassis of a vehicle. As the vehicle moves, the turntable of the retarder is radiated by the air flow due to the rotation; thus, the radiator system of the retarder can be simplified separately. As shown in Fig. 1, the turntable is divided into inner and outer parts. The inner ring is connected to the force bearing of the retarder and flange through a connecting plate, and the torque generated by the retarder is transmitted to the transmission shaft to decelerate the vehicle. The outer ring section consists of a thick metal disk and radiating spokes. The main function of the thick disk is to generate eddy currents and braking torque and dissipate heat through the spokes.

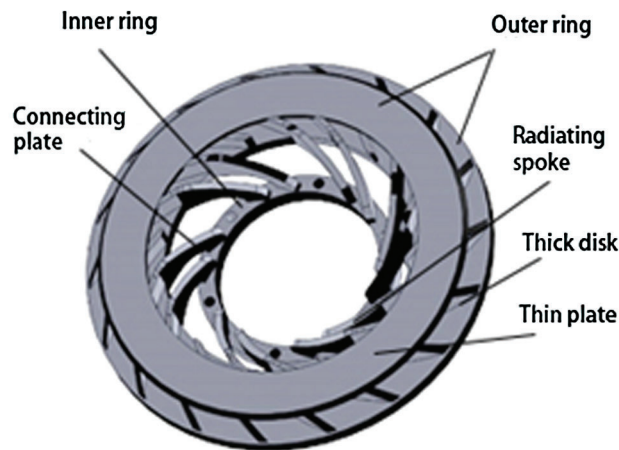


Figure 1: Turntable model

As the retarder rotates, the pressure difference generated in the air at adjacent locations leads to air convection. The air pressure on the windward side increases and that on the leeward side decreases during the rotation of the radiating spokes and the connecting plate on the turntable, thereby generating air flow. Because of the limitation of the sheet portion, air flows from the inside to the outside through the passage between the ribs as the turntable rotates.

To improve the air convection state of the retarder, its structure was modified. As shown in Fig. 2, the conventional retarder turntable is taken as the reference type, and the modified design is the control type. The following are the differences in the design of the control-type turntable:

(1) The two turntables have different vane shapes. The reference-type turntable has an involute-shape vane, and the connecting rib with the inner ring has a tangential form. The control-type turntable has a circular arc-shaped vane, designed to reduce the air intake resistance and increase the air intake volume as the turntable rotates.

(2) The two turntables have different edge angles, to change the air flow turbulence condition due to the angle of the air outlet. The control-type turntable has a higher edge angle.

(3) There are 24 heat sinks in the reference-type turntable while 16 in the control-type turntable.

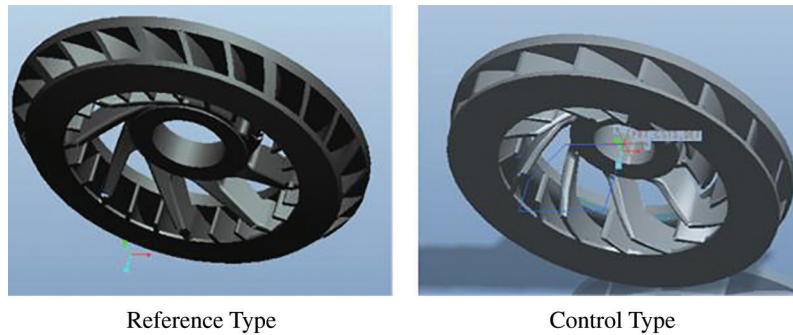


Figure 2: Structures of retarder turntables

3.2 Calculation Method

3.2.1 Control Equations

In this study, air is assumed to be a continuous medium, an incompressible ideal gas. For example, density, velocity, and pressure are regarded as continuous functions of space. The characteristics of the model can be described by mass continuous condition, momentum conservation, and energy balance condition [17,18].

1. Mass balance equation

The mass balance equation is also called continuity equation.

In view of coordinate space, if we take the finite volume τ bounded by S -plane, then we denote S -plane as the control surface and τ as the control body. Take the external normal direction as the positive direction of the normal and \mathbf{n} as the unit vector of the external normal direction. Considering the change of fluid mass in the volume, the change is mainly caused by the following two reasons:

(1) There is fluid flowing out or in through S -plane, and the total change of flow out and in per unit time is as follows:

$$\int_S \rho v_n dS = \int_S \mathbf{n} \cdot \rho \mathbf{v} dS \quad \underline{\text{Gauss formula}} \quad \int_\tau \text{div}(\rho \mathbf{v}) d\tau \quad (7)$$

(2) Owing to the unsteady density field, the mass of volume τ will change in unit time by

$$- \int_\tau \frac{\partial \rho}{\partial t} d\tau \quad (8)$$

The two should be equal; thus,

$$\int_\tau \text{div}(\rho \mathbf{v}) d\tau = - \int_\tau \frac{\partial \rho}{\partial t} d\tau \quad (9)$$

As volume τ is arbitrary and the integrand function is continuous,

$$\frac{\partial \rho}{\partial t} + \text{div}(\rho \mathbf{v}) = 0 \quad (10)$$

For incompressible fluid flow, the density ρ is constant. The continuity equations can be simplified as:

$$\operatorname{div} \mathbf{v} = 0 \quad (11)$$

2. Momentum equation

Take any fluid whose volume is τ , and its boundary is S . According to the theorem of momentum, the change fluid momentum in volume τ is equal to the sum of mass force and surface force (stress) acting on the volume.

If the surface force per unit area is $\mathbf{p}_n = \mathbf{n} \cdot \mathbf{P}$ (\mathbf{P} is the stress tensor), and the mass force per unit mass is \mathbf{F} , then the mass force and surface force acting on the volume are respectively

$$\int_{\tau} \rho \mathbf{F} d\tau \quad (12)$$

and

$$\int_S \mathbf{p}_n dS = \int_S \mathbf{n} \cdot \mathbf{P} dS \quad \text{Gauss formula} \quad \int_{\tau} \operatorname{div} \mathbf{P} d\tau \quad (13)$$

The change of momentum is

$$\frac{D}{Dt} \int_{\tau} \rho \mathbf{v} d\tau = \int_{\tau} \frac{D(\rho \mathbf{v})}{Dt} d\tau + \int_{\tau} \rho \mathbf{v} \frac{D}{Dt} d\tau \quad (14)$$

From continuity equation, we obtain

$$v_i \frac{\partial \rho}{\partial t} + v_i \operatorname{div}(\rho \mathbf{v}) = v_i \left(\frac{\partial \rho}{\partial t} + \operatorname{div}(\rho \mathbf{v}) \right) = 0 \quad (15)$$

where v_i is the speed in each direction.

The momentum equation is then

$$\frac{\partial(\rho v_i)}{\partial t} + \operatorname{div}(\rho v_i \mathbf{v}) = \rho \left(\frac{\partial v_i}{\partial t} + \mathbf{v}_i \cdot \operatorname{grad} v_i \right) \quad (16)$$

The above equations are the motion equations of viscous fluid expressed by stress, and they are applicable to any viscous fluid and any motion state.

In general, we make the following assumptions. (1) The stress tensor of the moving fluid should tend to the stress tensor of the static fluid after the motion stops. (2) The relation between the stress tensor and deformation rate tensor is a linear homogeneous function. (3) The fluid is isotropic, that is, the fluid property does not depend on the direction or transformation of the coordinate system. On applying generalized Newton's law, the momentum equation of compressible fluid can be obtained as follows:

$$\begin{cases} \frac{\partial(\rho u)}{\partial t} + \operatorname{div}(\rho u \mathbf{v}) = \operatorname{div}(\mu \operatorname{grad} u) - \frac{\partial p}{\partial x} + S_u \\ \frac{\partial(\rho v)}{\partial t} + \operatorname{div}(\rho v \mathbf{v}) = \operatorname{div}(\mu \operatorname{grad} v) - \frac{\partial p}{\partial y} + S_v \\ \frac{\partial(\rho w)}{\partial t} + \operatorname{div}(\rho w \mathbf{v}) = \operatorname{div}(\mu \operatorname{grad} w) - \frac{\partial p}{\partial z} + S_w \end{cases} \quad (17)$$

where u, v, w are the velocity components in x, y, z directions respectively and p is the pressure.

The generalized source term is defined as

$$S_u = \rho F_x + s_x, S_v = \rho F_y + s_y, S_w = \rho F_z + s_z \quad (18)$$

When the viscosity of the fluid is constant and incompressible (Newtonian fluid), there are

$$s_x = \frac{\partial}{\partial x} \left(\mu \frac{\partial u}{\partial x} \right) + \frac{\partial}{\partial y} \left(\mu \frac{\partial v}{\partial x} \right) + \frac{\partial}{\partial z} \left(\mu \frac{\partial w}{\partial x} \right) = 0 \quad (19)$$

As the fluid is assumed to be isotropic, there are similar conclusions in the Y and Z directions with the above x directions.

Then, the motion equation of incompressible flow can be obtained as follows:

$$\begin{cases} \frac{\partial u}{\partial t} + \text{div}(u\mathbf{v}) = \text{div}(v\text{grad}u) - \frac{1}{\rho} \frac{\partial p}{\partial x} + F_x \\ \frac{\partial v}{\partial t} + \text{div}(v\mathbf{v}) = \text{div}(v\text{grad}v) - \frac{1}{\rho} \frac{\partial p}{\partial y} + F_y \\ \frac{\partial w}{\partial t} + \text{div}(w\mathbf{v}) = \text{div}(v\text{grad}w) - \frac{1}{\rho} \frac{\partial p}{\partial z} + F_z \end{cases} \quad (20)$$

where ν denotes the kinematic viscosity and momentum diffusion coefficient.

3. Energy equation

According to the law of energy conservation, in volume τ , the conversion rate of energy of fluid is equal to the work done by mass force and surface force in unit time plus the heat given to volume τ in unit time.

The sum of kinetic energy and internal energy of the fluid in volume τ is

$$\int_{\tau} \rho \left(U + \frac{V^2}{2} \right) d\tau \quad (21)$$

where U is the internal energy of the fluid per unit volume. The work done by mass force to the fluid in volume τ (\mathbf{v} is the movement distance in unit time) is

$$\int_{\tau} \rho \mathbf{F} \cdot \mathbf{v} d\tau \quad (22)$$

The work done by the surface force to the fluid in volume τ is

$$\int_S \mathbf{p}_n \cdot \mathbf{v} dS \quad (23)$$

The heat transmitted to the volume τ through the surface S in the form of heat conduction in unit time is

$$\int_S k \frac{\partial T}{\partial n} dS \quad (24)$$

The total amount of heat transferred into the volume τ in unit time due to radiation or other reasons (reaction, evaporation, among others) is

$$\int_{\tau} \rho q d\tau \quad (25)$$

where q is the heat distribution function of the unit mass.

From Eqs. (21)–(24), the energy conservation equation in integral form can be obtained as follows:

$$\frac{D}{Dt} \int_{\tau} \rho \left(U + \frac{V^2}{2} \right) d\tau = \int_{\tau} \rho \mathbf{F} \cdot \mathbf{v} d\tau + \int_S \mathbf{p}_n \cdot \mathbf{v} dS + \int_S k \frac{\partial T}{\partial n} dS + \int_{\tau} \rho q d\tau \quad (26)$$

For compressible fluids, the energy equation is

$$\frac{\partial(\rho T)}{\partial t} + \text{div}(\rho \mathbf{v} T) = \text{div} \left(\frac{k}{c_p} \text{grad} T \right) + \frac{S_T}{c_p} \quad (27)$$

For incompressible fluids, the energy equation is

$$\frac{\partial T}{\partial t} + \text{div}(\mathbf{v} T) = \text{div} \left(\frac{k}{\rho c_p} \text{grad} T \right) + \frac{S_T}{\rho c_p} \quad (28)$$

where k is thermal conductivity, c_p is specific heat capacity, and S_T is the source item.

In the above equations, the source term S_T consists of two parts: S_h , which is the external volume heat source; ϕ , which represents the production of internal energy due to viscous stresses.

S_T is defined as follows:

$$S_T = S_h + \phi \quad (29)$$

$$\phi = \mu \left\{ 2 \left[\left(\frac{\partial u}{\partial x} \right)^2 + \left(\frac{\partial v}{\partial y} \right)^2 + \left(\frac{\partial w}{\partial z} \right)^2 \right] + \left(\frac{\partial v}{\partial x} + \frac{\partial u}{\partial y} \right)^2 + \left(\frac{\partial w}{\partial y} + \frac{\partial v}{\partial z} \right)^2 + \left(\frac{\partial u}{\partial z} + \frac{\partial w}{\partial x} \right)^2 \right\} \quad (30)$$

where, μ is the viscosity.

For incompressible flows, the order of magnitude of ϕ is negligible with respect to the other terms and for that reason it can be ignored [19]. In addition, there is no external volume heat source in the simulation, so $S_h = 0$. Therefore, the source term is disregarded in our simulation.

3.2.2 Calculation Model of Retarder Turntable

The main numerical simulation methods for turbulence include direct simulation, large eddy simulation, and Reynolds time-averaged equation simulation. A direct simulation requires considerable memory and computing speed, and large eddy simulation is time-consuming. Therefore, the Reynolds time-averaged equation with the standard k - ε two-equation model is used in this study owing to its high calculation efficiency.

The objective of this study was to simulate the influence of two types of turntables on the air velocity. Because the air flowing is ambient air, the fluid is assumed to be an ideal gas. This is done to simulate the state of air flow in the turntable with the maximum accuracy possible.

For incompressible turbulent flows, the Reynolds averaged Navier-Stokes equations can be written in conservative form as follows [20]:

$$\frac{\partial \mathbf{v}}{\partial t} + \mathbf{v} \cdot \text{grad} \mathbf{v} = -\text{grad} p + \text{div}((\nu + \nu_T)[\text{grad} \mathbf{v} + \text{grad} \mathbf{v}^T]) \quad (31)$$

$$\text{div} \mathbf{v} = 0$$

where the kinematic viscosity ν depends only on the physical properties of the fluid, while ν_T is the turbulent eddy viscosity which is supposed to emulate the effect of unresolved velocity fluctuations \mathbf{v}' .

The standard k - ε model is based on the assumption that $\nu_T = C_\mu \frac{k^2}{\varepsilon}$, where k is the turbulent kinetic energy and ε is the dissipation rate. Hence, the PDE system is to be complemented by two additional convection-diffusion-reaction equations for computation of k and ε

$$\frac{\partial k}{\partial t} + \text{div} \left(k \mathbf{v} - \frac{\nu_T}{\sigma_k} \text{grad} k \right) = P_k - \varepsilon \quad (32)$$

$$\frac{\partial \varepsilon}{\partial t} + \text{div} \left(\varepsilon \mathbf{v} - \frac{\nu_T}{\sigma_\varepsilon} \text{grad} \varepsilon \right) = \frac{\varepsilon}{k} (C_1 P_k - C_2 \varepsilon) \quad (33)$$

where, $P_k = \frac{\nu_T}{2} |\text{grad} \mathbf{v} + \text{grad} \mathbf{v}^T|^2$ and ε are responsible for production and dissipation of turbulent kinetic energy, respectively.

In the calculation, the related parameters are shown in [Tab. 1](#).

Table 1: Values of constants in the calculation model

Near-wall treatment	Standard wall functions
C_μ	0.09
$c_{\varepsilon 1}$	1.44
$c_{\varepsilon 2}$	1.92
σ_k	1.0
σ_ε	1.3

3.2.3 Numerical Method

In this study, assuming that the gas flow is incompressible, the SIMPLE method (semi-implicit method for pressure linked equations) is used to solve the Navier–Stokes equation, proposed by Patankar et al. [21]. The steps of the algorithm are as follows:

- (1) Assume a velocity initial condition for calculating the coefficients and constants in the momentum discrete equation of the first iteration.
- (2) Assume a pressure field.
- (3) Calculate the coefficients and constants in the momentum discrete equation.
- (4) Solve the momentum discrete equation.
- (5) Solve the pressure correction equation according to the speed.
- (6) Correct the pressure and speed.
- (7) Solve all other discrete transport equations.
- (8) Repeat the iteration until the model converges.

Specifically, the numerical scheme is as [Tab. 2](#):

Table 2: Numerical schemes for the SIMPLE method

Item	Method
Gradient	Green–Gauss Cell based
Pressure	Second Order
Momentum	Second–Order Upwind
Turbulent Kinetic Energy	Second–Order Upwind
Turbulent Dissipation Rate	Second–Order Upwind

3.3 Finite Element Model

A finite element model is established based on the actual operating conditions of the retarder (Fig. 3). The structural model of the turntable includes two parts: a thick plate as the heat source and a heat sink. The fluid model is set up based on the structural model.

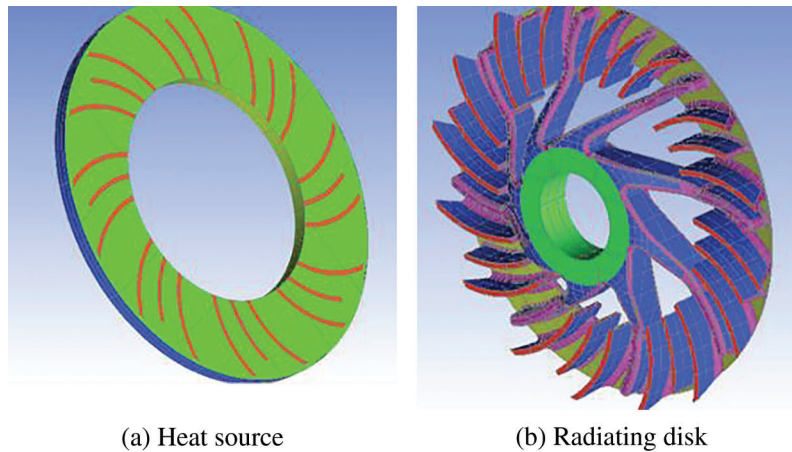


Figure 3: Finite element model of a solid model. (a) Heat source and (b) Radiating disk

The finite element model consists of two parts: a solid model and a fluid model. The solid model has a rotation domain and a far-field domain; the rotation domain is a disk-shaped region of radius 0.315 m in the vicinity of the turntable, and the far-field domain is a region of radius 1.5 m and 0.5 m in the axial direction.

The fluid model is divided into three parts: input, output, and middle parts. The middle part is where the air flows in the rotor disk, which will be investigated in this study. The fluid model is divided into three parts because the internal structure of the turntable is relatively complex, and the mesh quality is not ideal when the expansion method is used for mesh generation. Thus, we separate the middle layer and provide a more intensive mesh (Fig. 4).

To consider the calculation accuracy and efficiency, we performed a sensitivity analysis of the grids in the middle layer (Tab. 3). When the number of nodes reaches 871025 (No. 2), the settlement result of the outlet velocity will not change significantly. To improve the computational efficiency, the second group of grids is selected as the computational grid.

Tab. 4 lists the specific numbers of nodes and grids.

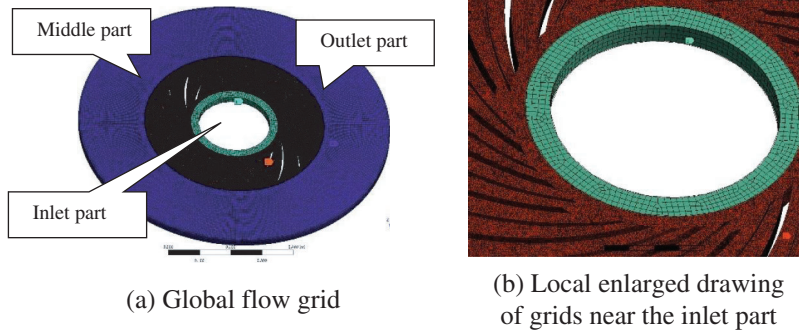


Figure 4: Finite element model of a fluid model. (a) Global flow grid and (b) Local enlarged drawing of grids near the inlet part

Table 3: Mesh sensitivity analysis

Serial number	Nodes	Relative change in outlet flow velocity (%)
1	156378	–
2	378953	0.4
3	489663	0.1
4	871025	0.05
5	1532711	0.05

Table 4: Data related to grids

Part	Nodes	Elements
Inlet part	3635	2380
Middle part	871,025	4,718,678
Outlet part	108,888	88,670

3.4 Boundary Conditions

(1) Turbulent state

Because turbulence is formed by a transition at some distance behind the entrance, the turbulence conditions are set at the boundary. The internal flow problem was overcome by appropriately setting the turbulence intensity at the inlet, which depends on the upstream flow state. In this study, the effect of the turntable structure on the airflow is investigated under ideal conditions. Therefore, it is assumed that the upstream flow is undisturbed, and the turbulence intensity at the inlet is thus relatively low at 1%.

(2) Heat generation rate

The braking torque of the eddy current retarder for stable braking is approximately 400 N·m. The braking power can be calculated using the torque power equation:

$$P = T \cdot n / 9.55 = 33507.9W \quad (34)$$

where P, T, and n denote the braking power, braking torque, and rotational speed, respectively.

According to the law of conservation of energy, the braking power of the retarder in the braking process of the vehicle is equal to the power generated by the heating part of the thick disk. Therefore, it can be calculated as follows:

$$\text{Heat generation rate of turntable} = \text{braking power/thick disc volume} = 11.6 \times 10^6 \text{ W/m}^3.$$

Tab. 5 lists the boundary conditions.

Table 5: Boundary conditions

Heat generation rate of turntable		$11.6 \times 10^6 \text{ W/m}^3$
Import and export boundaries		Opening boundary condition
Wall boundary		Adiabatic conditions
Internal interface		GGI connection mode
Materials	Fluid part	Ideal gas (compressible)
	Solid part	Steel surface emissivity: 0.8, diffusion fraction: 1.0

3.5 Overall Condition of Temperature and Flow Field Distribution

3.5.1 Reference-Type Turntable

As shown in Fig. 5a, when the reference-type turntable operates stably, the maximum temperature is 1021°C, and the maximum temperature on the flange surface is 345°C. Because the adiabatic wall boundary set in the numerical calculation ignores the radiant heat flow in the actual operation, the calculated maximum temperature is slightly higher than the actual maximum temperature. Fig. 5b shows the distribution conditions of the 3D air flow field during the operation of the existing turntable. The maximum velocity of air is approximately 25.76 m/s, and many turbulence phenomena exist on the inner side and outer edge of the turntable.

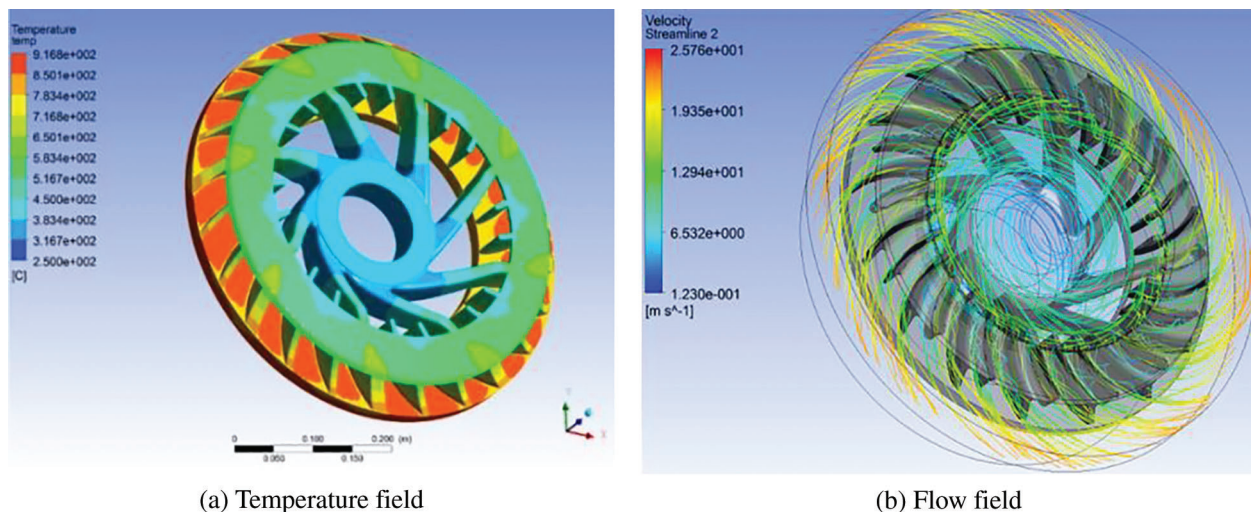


Figure 5: Numerical analysis results of reference turntable. (a) Temperature field and (b) Flow field

3.5.2 Control-Type Turntable

As shown in Fig. 6a, the maximum temperature for a stable operation of the control-type turntable is 917°C , and the maximum temperature on the flange surface is 322°C . The maximum temperature of the reference-type turntable is higher than that of the control-type turntable by 104°C , and the maximum temperature of the flange surface is higher than that of the control-type turntable by 23°C . Fig. 6b shows the 3D flow field of air during the operation of the turntable. As shown, the maximum flow velocity of air is approximately 41.13 m/s , the streamline graph is relatively uniform, and no excess turbulence is observed.

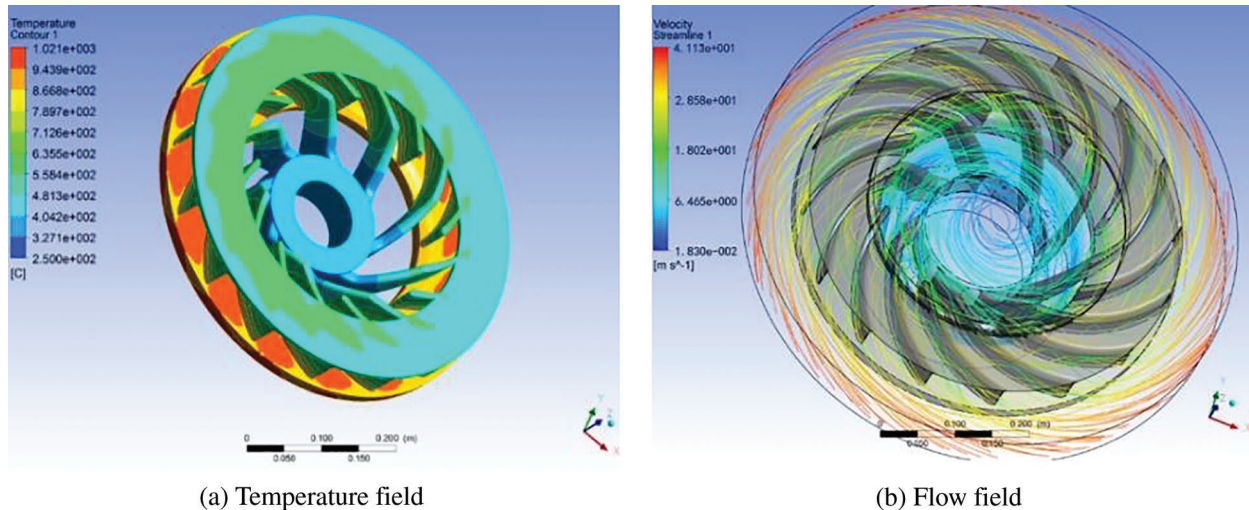


Figure 6: Numerical analysis results of control-type turntable. (a) Temperature field and (b) Flow field

3.5.3 Comparison of Analysis Results

The 3D flow fields of air during the working of the turntable before and after the design improvement are compared. The comparison results show that the overall flow velocity of the reference-type turntable is lower than that of the control-type turntable, with the former exhibiting more turbulence on the inner side and outer edge of the turntable than on the control-type turntable. The overall velocity of the flow field of the control-type turntable is higher than that of the reference-type turntable, and the streamline diagram is more uniform without high turbulence. From the perspective of heat transfer, the performance of turbulent flow is higher than that of laminar flow. However, the turbulent heat transfer is concentrated between the inner walls of the rotor, i.e., the high heat transfer performance is prominent only inside the retarder. The high-efficiency heat transfer owing to laminar flow carries the heat generated by the turntable away from the retarder and improves the overall heat dissipation performance. The results of temperature field analysis before and after the improvement of the turntable show that the maximum temperature of the reference-type turntable is higher than that of the control-type turntable by 104°C , and the maximum temperature of the flange surface of the reference-type turntable is lower than that of the flange surface of the control-type turntable by 23°C .

4 Validation Experiments

To verify the cooling effect of the reference-type and control-type turntables, we designed a wind speed test platform to experimentally test the eddy current turntable.

4.1 Test Method

1. Install the control-type rotor sub-assembly (stator is not installed) on the test bench in the working condition, start the test bench and set the rotational speed to 1045 rpm, and record the wind speed near the highest point. Fig. 7 shows the settings of the wind speed tester; its position remains the same in all tests.

The motor is a variable-frequency adjustable-speed three-phase induction motor (Changsha Motor Factory Co., Ltd.). Tab. 6 lists the main parameters of the motor.

Tab. 7 lists the main parameters of the wind speed sensor (Shenzhen Jetronl Instruments Co., Ltd.).



Figure 7: Settings of air speed tester for control-type retarder

Table 6: Parameters of motor

Rated frequency	50 Hz
Nominal power	500 kW
Rated voltage	380 V
Protection grade	IP44
Cooling method	IC81W6
Installation type	IMB3

Table 7: Parameters of wind speed sensor

Measuring range	0.4–60 m/s
Temperature in the operating environment	0–60°C
Operating humidity	<80% RH
Host size	177 mm × 64 mm × 32 mm
Probe diameter	72 mm
Probe length	220 mm

2. Adjust the rotation speed to 2000 rpm, measure the torque, power, and wind speed following Step 1, and record the same.

3. After testing the control-type turntable, remove it and install the reference-type rotor assembly, because the structure of the reference-type turntable is different from that of the control-type turntable, to ensure that the distance between the two types of turntables and the wind speed tester is the same (Figs. 8 and 9).

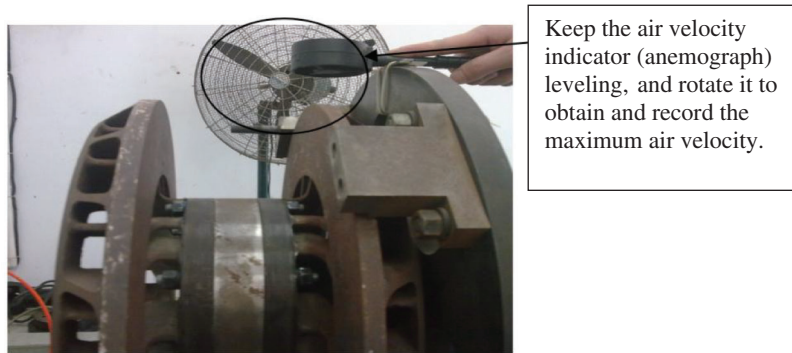


Figure 8: Settings of air speed tester for the reference-type retarder



Figure 9: Supported position of air speed tester in the control-type retarder's radiator system

4. After testing the reference-type turntable, remove and start the test bench, idle at 1000 and 2000 rpm, and record the initial torque.

5. Repeat Steps 1–4 five times and shut down after cooling.

4.2 Experimental Data

Based on the experimental results obtained under the actual working condition at 1045 rpm (Tab. 8 and Fig. 10), the average air velocity is increased from 22.88 to 38.8 km/h. The air velocity of the control-type turntable is nearly twice that of the reference-type turntable. Additionally, the results of each test show that the wind speed is stable under the specified conditions.

As shown in Tab. 9 and Fig. 11, when the rotational speed is increased to 2095 rpm, the air velocity is doubled, and the test results are stable.

Table 8: Measured value of air velocity at a rotational speed of 1045 rpm

Test No.	Air Velocity (km/h)	
	Reference type	Control type
1	23.0	40.0
2	22.9	39.7
3	23.1	38.1
4	22.5	38.5
5	22.9	37.7
Average	22.88	38.8

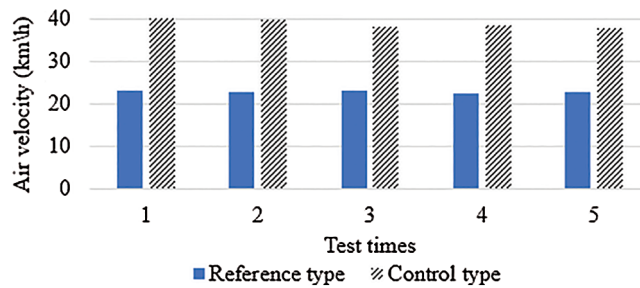


Figure 10: Comparison of tested air velocity at a rotational speed of 1045 rpm

Table 9: Measured value of air velocity at a rotational speed of 2095 rpm

Test No.	Air Velocity (km/h)	
	Reference type	Control type
1	47.1	83.5
2	47.9	82.5
3	47.3	83.4
4	47.2	83.7
5	47.2	84.3
Average	47.34	83.48

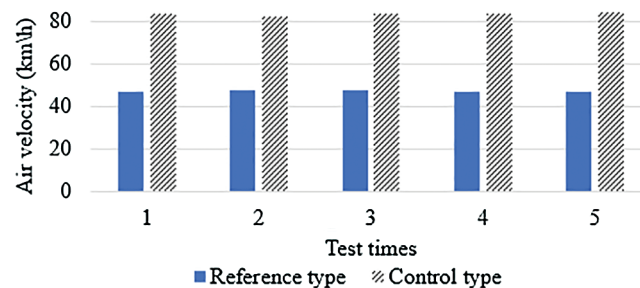


Figure 11: Comparison of tested air velocity at a rotational speed of 2095 rpm

4.3 Data Evaluation

The data obtained from the test indicate that the air velocity of the control-type turntable is higher than that of the reference-type turntable. Further, at rotational speeds of 1045 and 2095 rpm, the air velocity of the control-type turntable is respectively 1.69 and 1.76 times that of the reference-type turntable. The control-type turntable significantly improves the convective heat transfer capacity of the retarder, thus validating the above numerical analysis.

The objective of the numerical simulation is to provide a reference for the mechanical design of the rotary table. Some differences do exist between the experimental and numerical simulation results. The numerical simulation was conducted to understand the influence of the mechanical model on the flow field. This simulation process under an ideal situation considers only the ambient temperature of the ideal gas and the speed and pressure of the airflow at the inlet and outlet. However, many unavoidable interference factors are involved in the experiment due to material inhomogeneity, such as environmental vibration, temperature gradient, acceleration and deceleration, and rotational vibration. The experimental results show that the difference between the wind speed simulation results (25.76 m/s) and the experimental results (22.88 m/s) for the reference-type turntable is approximately 11%, whereas the difference between the wind speed simulation results (41.13 m/s) and the experimental results (47.34 m/s) for the control-type turntable is approximately 15%. This difference is considered acceptable.

5 Conclusion

In this study, numerical and experimental analyses were conducted on a reference-type turntable and a control-type turntable of an eddy current retarder. The following results were obtained:

- (1) The structure of the retarder turntable has a significant influence on the convective heat transfer of the retarder. Compared with an involute-type blade, an arc-type blade has a better air flow guiding effect, and the air flow field changes from turbulent flow to laminar flow. The results of numerical analysis showed that the maximum temperature of the control-type turntable is lower than that of the reference-type turntable. Furthermore, there is no local high temperature, and the temperature field is more uniform along the circumferential direction.
- (2) The air velocity of the turntable was measured by experimental analysis. The results showed that the speed of the control-type turntable is 1.69 and 1.76 times that of the reference-type turntable at 1045 and 2095 rpm, respectively, demonstrating that this turntable can significantly improve the convective heat transfer capacity of the retarder.

Funding Statement: This paper was supported by Scientific and Technological Research Program of Chongqing Municipal Education Commission (Grant No. KJ1603004).

Conflicts of Interest: The authors declare that they have no conflicts of interest to report regarding the present study.

References

1. Tirovic, M., Sergent, N., Campbell, J., Roberts, P., Vignjevic, R. (2012). Structural analysis of a commercial vehicle disc brake caliper. *Proceedings of the Institution of Mechanical Engineers, Part D: Journal of Automobile Engineering*, 226(5), 613–622. DOI 10.1177/0954407011423447.
2. Christoforou, Z. D., Karlaftis, M. G., Yannis, G. (2010). Heavy vehicle age and road safety. *Proceedings of the Institution of Civil Engineers-Transport*, 163(1), 41–48. DOI 10.1680/tran.2010.163.1.41.
3. Ergun, R. E., Ucar, M., Ertunc, H. M., Cengiz, A. (2014). A development of electromagnetic retarder controller to stabilise vehicle speed by using PWM technique. *International Journal of Heavy Vehicle Systems*, 21(2), 169–181. DOI 10.1504/IJHVS.2014.061653.

4. Jiao, B. F., Li, D. S., Du, X., Zhang, K. (2014). Performance analysis and experimentation of a liquid-cooled eddy current retarder with a dual salient poles design. *IEEE Transactions on Energy Conversion*, 29(1), 84–90. DOI 10.1109/TEC.2013.2288695.
5. Xi, Z. L., Sheng, L. D., Lei, Y. W. (2014). Study on influence factor of braking torque in liquid-cooled eddy current retarder with a structure of two salient poles. *Journal of Chemical and Pharmaceutical Research*, 6(5), 1135–1141.
6. Ye, L. Z., Liu Y. P., Cao, M. G., Li, D. S. (2018). Braking characteristics and experiment of a permanent magnet eddy-current retarder. *Journal of Beijing University of Technology*, 44(6), 837–842.
7. Natarajan, N., Krishnaraj, V., Davim, J. P. (2015). Fabrication of experimental set-up and testing. In: *Metal Matrix Composites. SpringerBriefs in Applied Sciences and Technology*. Cham, Switzerland: Springer. DOI 10.1007/978-3-319-02985-6_4.
8. Chunbao, L., Dong, X., Wenxing, M., Zhe, Y., Xuesong, L. (2015). Analysis of unsteady rotor–stator flow with variable viscosity based on experiments and CFD simulations. *Numerical Heat Transfer, Part A: Applications*, 68(12), 1351–1368. DOI 10.1080/10407782.2015.1052298.
9. Gulbahce, M. O., Kocabas, D. A., Nayman, F. (2013). Investigation of the effect of pole shape on braking torque for a low power eddy current brake by finite elements method. *The 2013 8th International Conference on Electrical and Electronics Engineering*, pp. 28–30, Piscataway.
10. Jin, L. (2017). *Heat dissipation research of a kind of current-eddy retarder. (Master of Engineering)*. Shenzhen, China: Harbin Institute of Technology.
11. Zheng, H. P., Lei, Y. L., Song, P. X. (2017). Hydraulic retarders for heavy vehicles: analysis of fluid mechanics and computational fluid dynamics on braking torque and temperature rise. *International Journal of Automotive Technology*, 18(3), 387–396. DOI 10.1007/s12239-017-0039-z.
12. Nonino, C., Savino, S., Del Giudice, S. (2015). FEM for the 3-D analysis of conjugate conduction-convection heat transfer in cross-flow micro heat exchangers. *International Journal of Numerical Methods for Heat & Fluid Flow*, 25(6), 1322–1339. DOI 10.1108/HFF-07-2014-0232.
13. Kachi, S., Bensouici, F. Z., Ferroudj, N., Boudebous, S. (2019). Effect of Richardson number on unsteady mixed convection in a square cavity partially heated from below. *Fluid Dynamics & Materials Processing*, 15(2), 89–105. DOI 10.32604/fdmp.2019.00263.
14. Hartman, J. (2014). *Effects of velocity, temperature and rainfall on the friction coefficient of pneumatic tyres and bitumen roads. (Ph.D. Thesis)*. Melbourne, Australia: RMIT University.
15. Bentarzi, F., Mataoui, A. (2018). Turbulent flow produced by twin slot jets impinging a wall. *Fluid Dynamics and Materials Processing*, 14(2), 107–120.
16. Frulla, G., Gili, P., Visone, M., D’Orlando, V., Lappa, M. (2015). A practical engineering approach to the design and manufacturing of a mini kW bladewind turbine: definition, optimization and CFD analysis. *Fluid Dynamics and Materials Processing*, 11(3), 257–277.
17. Lappa, M. (2012). *Rotating thermal flows in natural and industrial processes*. Chichester, England: John Wiley & Sons, Ltd.
18. Tao, W. Q. (1991). *Computational fluid dynamics and heat transfer*. Beijing: China Architecture & Building Press.
19. Deyi, S. (2006). *Free convection film flows and heat transfer: models of laminar free convection with phase change for heat and mass transfer analysis*. Berlin, Heidelberg: Springer.
20. Kuzmin, D., Mierka, O., Turek, S. (2007). On the implementation of the k- ϵ turbulence model in incompressible flow solvers based on a finite element discretisation. *International Journal of Computing Science Mathematics*, 1(2–4), 193–206.
21. Patankar, S. V., Spalding, D. B. (1972). A calculation procedure for heat, mass and momentum transfer in three-dimensional parabolic flows. *International Journal of Heat and Mass Transfer*, 15(10), 1787–1806. DOI 10.1016/0017-9310(72)90054-3.